

A Lightweight and Detector-free 3D Single Object Tracker on Point Clouds

Yan Xia^{1†} Qiangqiang Wu^{2†} Tianyu Yang³ Wei Li⁴ Antoni B. Chan² Uwe Stilla¹

¹Technical University of Munich ²City University of Hong Kong ³Tencent AI Lab ⁴Inceptio X-Lab

Abstract

Recent works on 3D single object tracking treat the tracking as a target-specific 3D detection task, where an off-the-shelf 3D detector is commonly employed for tracking. However, it is non-trivial to perform accurate target-specific detection since the point cloud of objects in raw LiDAR scans is usually sparse and incomplete. In this paper, we address this issue by explicitly leveraging temporal motion cues and propose DMT, a Detector-free Motion prediction based 3D Tracking network that totally removes the usage of complicated 3D detectors, which is lighter, faster, and more accurate than previous trackers. Specifically, the motion prediction module is firstly introduced to estimate a potential target center of the current frame in a point-cloud free way. Then, an explicit voting module is proposed to directly regress the 3D box from the estimated target center. Extensive experiments on KITTI and NuScenes datasets demonstrate that our DMT, without applying any complicated 3D detectors, can still achieve better performance ($\sim 10\%$ improvement on the NuScenes dataset) and faster tracking speed (i.e., 72 FPS) than state-of-the-art approaches. Our codes will be released publicly.

1. Introduction

Single object tracking (SOT) in large-scale urban street environments is a key task in the field of computer vision, which has wide applications ranging from autonomous driving [17, 22] to robot vision [6, 23]. Given an initial bounding box of a template object in the first frame from images or LiDAR scans, the aim is to localize its location by identifying the trajectory across all frames. In the past decade, a variety of image-based trackers have shown promising performance. However, the performance of image-based methods often fail in degraded situations, e.g., when facing drastic lighting changes [27, 30]. As a possible remedy, 3D point clouds collected from LiDAR provide detailed depth and geometric information which is inherently invariant to lighting changes [38], making it more robust to perform track-

ing across frames taken from different illumination environments.

The main challenges of point cloud based single object tracking are three-fold: 1) point cloud is structurally unordered compared with images, and thus the network must be permutation-invariant [30]; 2) point cloud is incomplete because of occlusion or self-occlusion, and thus the network must be robust to different resolutions of input point clouds [39]; 3) The scanned point clouds of different objects might have highly similar shapes [45], and thus the network must be robust to shape ambiguities.

SC3D [10] is a pioneering 3D tracker, which first enriches geometric features from sparse point clouds using a shape completion network [1], and then executes template matching with target proposals generated by Kalman filtering [28]. However, SC3D is not an end-to-end network and cannot meet the real-time requirement. Towards these concerns, P2B [27] first calculates point-based correlation between the template and the search area, and then applies a siamese region proposal network (RPN) [19] to detect the final target proposal. Following this, BAT [45] explores the free box information to enhance the target-specific search feature. MLVSNet [33] proposes to perform voting on multi-level features to get more vote centers. With breakthroughs of transformer-based vision methods, the authors of PTT [30] introduce a transformer module to further refine the target-specific search feature. These methods all use the historical information to decide search area and sample seeds in a implicit strategy, and then apply the RPN module (VoteNet [26]) for detecting the target in the search space. Although this improves search results, the usage of RPN module is still complicated and may easily fail when the scanned point cloud is relatively sparse. Furthermore, the previous 3D trackers ignore one key point: *the coarse target center in the current frame can be directly predicted in a point-cloud free way by explicitly exploring the historical information. The predicted center can be further served as a strong prior knowledge for final 3D target box prediction.*

To fully utilize this prior knowledge, we propose a novel lightweight and detector-free 3D single object tracking network named DMT (Detector-free Motion prediction based 3D Tracking) network. Specifically, we first develop a mo-

[†]Equal contribution.

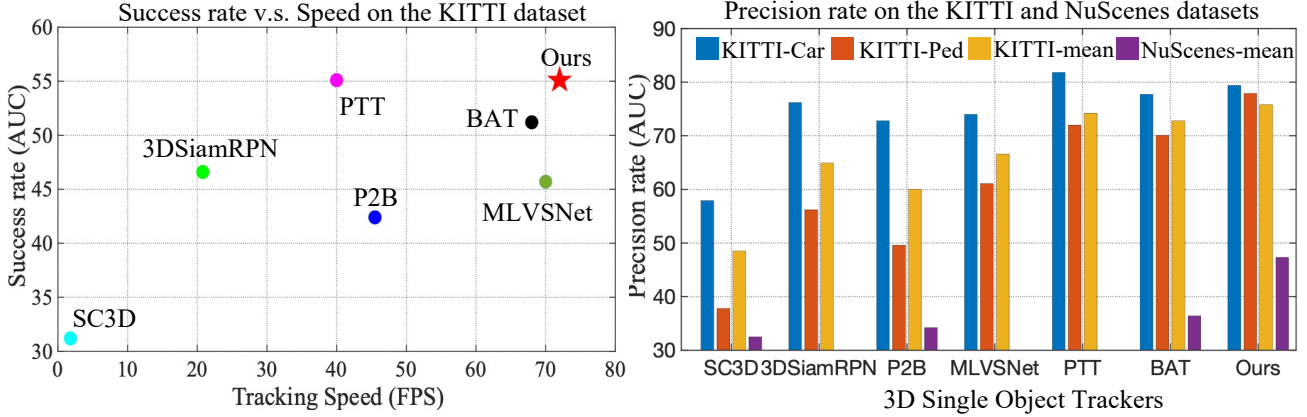


Figure 1. (Left) Tracking accuracy v.s. speed on the car category of KITTI benchmark. Our DMT outperforms state-of-the-art 3D single object trackers in terms of both tracking accuracy and speed. (Right) Precision comparison on KITTI-Car, KITTI-Pedestrian, KITTI-mean and NuScenes-mean.

tion prediction module to estimate the 3D coordinates of a potential target center in the current frame using previous frames. Although the estimated center is coarse, it can provide a strong prior information as guidance. Thus, we furthermore design an explicit voting layer only consisting of several multi-layer perceptron (MLP) layers to refine the target center with the desired position and rotation.

To summarize, the main contributions of this work are:

- To the best of our knowledge, we are the first to totally remove the usage of complicated 3D detectors or proposal generation in 3D single object trackers. We prove that object motion is a useful cue in 3D SOT, which allows for less complex tracking models, while still achieving state-of-the-art performance. Our method can be served as a simple yet strong baseline in the 3D SOT community.
- We propose a new lightweight and detector-free 3D single object tracking network based on motion prediction, called DMT, which purely applies on point clouds. With the guidance of center priors, an explicit voting module only consisting of several MLP layers is designed to generate the accurate 3D positions and rotation in X - Y plane.
- We conduct experiments on the KITTI [9] and NuScenes [5] benchmark datasets to demonstrate the superiority of DMT over other state-of-the-art 3D SOT methods, as shown in Fig. 1. Notably, the performance on the NuScenes datasets reaches $\sim 10\%$ improvement on average, while running faster and lighter than the previous state-of-the-art.

2. Related work

The goal of object tracking is to locate the object in successive frames using raw data collected from various sensors, which can be 2D images or 3D point clouds. Numerous methods for tracking objects in 2D or 3D spaces have been developed, which are divided into two categories based on the number of tracked objects: single object tracking (SOT) and multiple object tracking (MOT).

2D single object tracking. 2D SOT is a basic computer vision task with a long history spanning decades. The representative deep tracking framework in recent years is built on a deep Siamese network [3]. The pioneering work is SiamFC [3], which treats visual tracking as a general template matching problem and performs favorably in terms of both tracking performance and speed. Based on SiamFC, many improvements have been proposed. SiamDW [44] firstly adopts very deep neural networks (e.g., ResNet [12]) as backbone for Siamese tracking. To handle large scale appearance variations, SiamRPN [20] and SiamRPN++ [18] employ region proposal networks (RPNs) for scale regression. In addition, much efforts are made on building a robust target appearance model, including UpdateNet [42], MemTrack [40] and DSiam [11]. Recent progress on 3D SOT (e.g., P2B [27] and BAT [45]) follow a bounding box regression-based framework, which is mainly inspired from the 2D tracker SiamRPN. However, the data source in 3D tracking is totally different from the images used in 2D tracking. Directly regressing target bounding boxes is still limited when the scanned point clouds are sparse. In this work, we alleviate this problem by incorporating temporal and spatial tracking information for bounding box regression.

Motion prediction has also been explored in 2D object tracking in videos. However, 2D motion prediction is gener-

ally unreliable due to the scale changes, perspective effects, and inconsistent motion caused by viewing a 2D projection of an object moving in a 3D scene. Indeed, most modern deep trackers use a simple learning-free motion prior (e.g., cosine window in SiamFC), and instead rely on the more reliable 2D appearance features. There are a few 2D trackers that use the motion module to *assist* with object detection, e.g., motion-conditioned detection [14, 31, 46] for associating objects in consecutive frames and motion-guided multiple proposal generation [21, 32]. Notably, these trackers still require an object detector module (e.g. RPN) performing on a per-frame basis. In contrast to 2D SOT, we show that motion cues in 3D point cloud tracking are more reliable and can be exploited to build lightweight trackers that do not use complex detectors, while still achieving state-of-the-art performance.

3D single object tracking. Early 3D SOT methods [2, 4, 15, 16] generally rely on the RGB-D information and employ the 2D siamese tracking architecture. Though these methods are effective in certain situations, they do not fully explore 3D geometric clues due to a lack of 3D networks. SC3D [10] is a pioneering work for point cloud based tracking, which regularizes the latent spaces of template point cloud and search candidates using a shape completion network. However, this method is time-consuming since it uses Kalman filtering for target proposal generation. Moreover, it ignores the local geometric information of each target proposal. PSN [7] leverages 3D Siamese network for single person tracking. However, it cannot predict the orientation and size of the target. F-Siamese tracker [47] explores RGB images to produce 2D region proposals for reducing 3D point cloud searching space. However, its performance depends more on the 2D tracker. 3DSiamRPN [8] combines 3D Siamese network and 3D RPN to track a single object, but the one stage RPN network limits its performance. Recently, P2B [27] fuses the target object information into 3D search space and then adopts a state-of-the-art object detection network (VoteNet) to detect the target. Following this, BAT [45] proposes to add the bounding box information provided in the first frame as an additional cue. MLVS-Net [33] performs Hough voting on multi-level features for getting more vote centers. PTT [30] introduces the transformer architecture to enhance the target-specific feature extracted in P2B. However, these methods all use the RPN to regress the bounding box of the target, which is inspired by their 2D SOT counterparts [18, 20, 44]. In this paper, we show that complex detectors can be removed from 3D SOT by better leveraging more reliable 3D motion prediction, and still achieving state-of-the-art performance.

3D multiple object tracking. Different with SOT where the initial position is given in first frame, 3D MOT trackers adopt a detector to determine the number of objects in a sequence. The goal of 3D MOT is to associate these detected

objects in all frames. [29] detects and estimates the distance to objects using a single image, and then uses a Poisson multi-Bernoulli mixture tracking filter to achieve 3D tracking. [24, 25, 34] utilize Kalman filter to obtain the 3D motion cue for simplicity and efficiency. With breakthroughs of learning based 2D MOT methods, deep learning on 3D MOT tasks has drawn growing attention. [35, 43] explore 3D network to learn the 3D geometric characteristics and motion cues. Recently, [36] adopts feature consistency of objects in consecutive frames to improve the tracking accuracy.

3. Problem statement

Let $B_{init} = \{x, y, z, h, w, l, \theta\}$ be a known 3D bounding box of the object in the first frame, where (x, y, z) is the center coordinates of the 3D bounding box, (h, w, l) stands for the height, width, and length respectively, and θ is the orientation of the bounding box. And let $Q = \{Q_i\}_{i=1}^M$ be a query point cloud created by cropping and centering the object in the first frame with B_{init} . We define the single object tracking task as locating the same object in the search point cloud $P = \{P_i\}_{i=1}^N$ given the B_{init} frame by frame. Formally, previous state-of-the-art 3D single object trackers [27, 45] can be formulated as:

$$Tracker(Q, P, B_{init}) \rightarrow (\hat{x}, \hat{y}, \hat{z}, \hat{\theta}), \quad (1)$$

where $Q \in \mathbb{R}^{M \times 3}$, $P \in \mathbb{R}^{N \times 3}$ and $B_{init} \in \mathbb{R}^7$. Notably, we only predict the center coordinates and orientation $(\hat{x}, \hat{y}, \hat{z}, \hat{\theta})$ of the target since the height, width and length of this object will not be changed in other frames.

Previous trackers employ off-the-shelf detectors on scanned point clouds for target detection. They may easily drift when the point clouds are relatively sparse or incomplete. In this paper, we propose to predict the potential target center in a point-cloud free way, which fully explicitly leverages motion cues from previous target states $S_{prev} = \{S_1, S_2, \dots, S_{t-1}\}$. The state S_t is the predicted center coordinates in the t -th frame, and the whole process is formulated as:

$$Tracker(Q, P, B_{init}, \mathcal{M}(S_{prev})) \rightarrow (\hat{x}, \hat{y}, \hat{z}, \hat{\theta}), \quad (2)$$

where $\mathcal{M}(\cdot)$ is a motion prediction function that estimates a potential target center in the current frame based on previous target states.

4. Methodology

The overall network architecture of our DMT is shown in Fig. 2. Given the query and search point cloud with coordinates denoted as Q and P , we first use the backbone to

Algorithm 1 The Workflow of DMT

Input: Points Q in query, points P in search area, previous target states S_{prev} and target-specific search feature f .

- 1: **Potential target center generation.** Given S_{prev} , predict a coarse target center C_{coarse} in the current frame using a motion prediction module.
- 2: **Explicit voting.** Feed f and C_{coarse} into an explicit voting module to estimate the a target-specific point feature \hat{f} of the target center.
- 3: **Final box regression.** Regress the 3D bounding box of the target based on \hat{f} using a prediction head.

Output: The 3D bounding box of the target.

extract target-specific feature following [45]. Unlike previous studies, we propose a motion prediction module to estimate a potential target center in the current frame based on previous target states S_{prev} , with details described in Section 4.1. Afterwards, an explicit voting module is adopted to modify the coordinates of the coarse predicted center and predict the orientation in Section 4.2. The loss function is presented in Section 4.3. The training strategy and implementation details are explained in Section 4.4. For highlighting the simplicity of our method, we also sketch the detailed flow in Algorithm 1.

4.1. Motion prediction module

The previous end-to-end 3D SOT methods [27, 30, 45] heavily rely on point clouds features for target object detection. However, erroneous detection may occur when the point cloud of the target is sparse and/or incomplete. To alleviate this, we propose to explicitly leverage spatio-temporal information for 3D SOT. Specifically, we introduce a motion prediction module (MPM) \mathcal{M} based on previous target states (i.e., predicted 3D target center coordinates in the previous frames) to predict a coarse target center in the current frame. Suppose that we have a tracklet $\{(x_i, y_i, z_i)\}_{i=1}^t$ in the previous t frames, the prediction of the target center location in the next $(t + 1)$ -th frame is formulated as:

$$(\hat{x}_{t+1}, \hat{y}_{t+1}, \hat{z}_{t+1}) = \mathcal{M}(\{(x_i, y_i, z_i)\}_{i=1}^t). \quad (3)$$

In our general design, common regression or prediction models can be employed as our MPMs for effective target center prediction. Here we introduce several simple yet effective MPMs.

Constant velocity model. The constant velocity model assumes that the target acceleration in the current frame is 0 and the velocity of target in the current frame should be equal to the velocity in the last frame. Given the target locations in the $(t - 1)$ and t -th frames $\{(x_i, y_i, z_i)\}_{i=t-1}^t$, the predicted target center coordinate in the $(t + 1)$ -th frame is calculated as $(2x_t - x_{t-1}, 2y_t - y_{t-1}, 2z_t - z_{t-1})$. Despite

the simplicity of this model, we find that this simple model can also work very well in our DMT.

Sequence-to-sequence prediction model. The goal of our MPM is to predict a 3D coordinate based on previous estimated t target coordinates, which is actually a sequence-to-sequence prediction task. Long Short-Term Memory (LSTM) network [13] is a typical sequence-to-sequence prediction model that has been wisely used in various sequence prediction tasks. In this paper, we choose a multi-layer LSTM since this naive LSTM model can better validate the effectiveness of our proposed tracking method. The conventional LSTM cell is shown in Fig. 2. More details can be found in [13]. In the implementation, we select the center coordinates of the 10 consecutive frames from the time $t - 10$ to t to predict potential target center coordinates in the $(t + 1)$ -th frame. In the training stage, we prepare multiple training tracklets generated from the KITTI and NuScenes datasets to train the LSTM respectively. In online tracking, we directly use the offline learned LSTM network for motion prediction without further updating.

Regression model. Traditional learning-based regression models can also be employed as MPMs. In this paper, we try several basic regression models including linear regression, ridge regression, Gaussian processor regression and Ransac regression. The training for the above models are similar to the LSTM-based MPM, i.e., using the generated tracklet training data for training in an offline manner.

The above basic MPMs can roughly predict the potential target center coordinate based on the previous states. The prediction is not always reliable since the previous target states may be noisy (i.e., the predicted target center does not match the ground-truth), or the target changes position in an unexpected way. To alleviate this problem, we propose a lightweight explicit voting module to further refine the MPM prediction.

4.2. Explicit voting module

Before going to the details of our proposed explicit voting module (EVM), we give a short review on the RPN module (VoteNet) used by previous trackers [27, 30, 33, 45]. The architecture of VoteNet includes two aspects: 1) Hough voting to convert the search area seeds into possible target centers; and 2) cluster neighboring possible target centers to obtain the final target center. For generating the possible target centers, VoteNet estimates the coordinate offsets between each search seed and ground-truth target center, which aims to push the predicted possible target centers and ground-truth target center to be as close as possible. In our DMT, the above two steps can be removed since the coarse target center location in the current frame is provided by our MPM, which makes our method simpler and lighter.

After obtaining the coarse target center coordinate $(\hat{x}_{t+1}, \hat{y}_{t+1}, \hat{z}_{t+1})$ estimated by MPM and target-specific

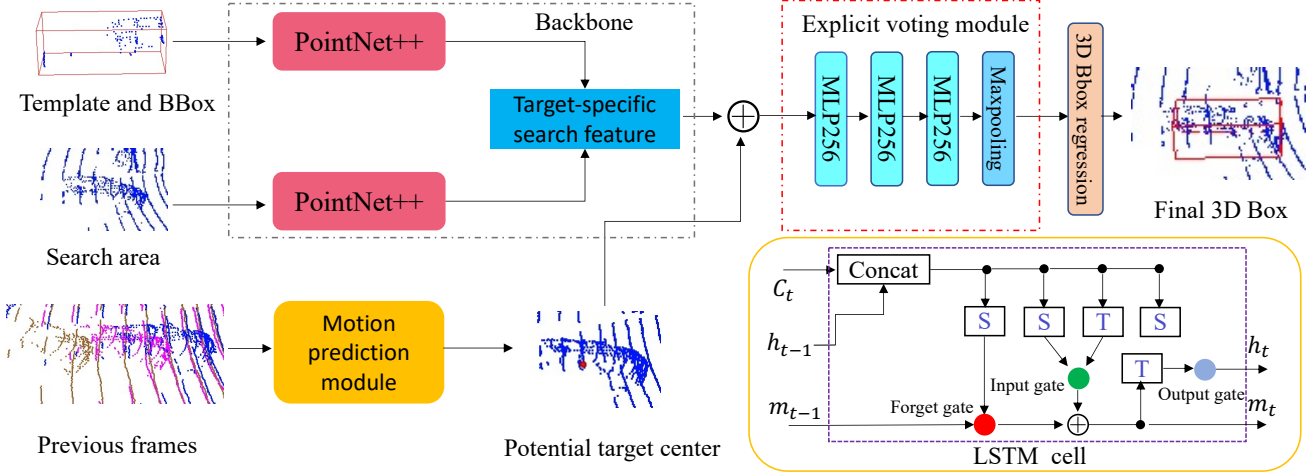


Figure 2. Overview of DMT. The motion prediction module (MPM) estimates the 3D coordinates of a potential target center. Next, the explicit voting module refines the target-specific search feature extracted by the backbone in [45] and the coarse predicted center. Finally, a 3D bounding box prediction head regresses the target location. One example of the MPM is an LSTM (lower right corner).

search seeds, the goal of our EVM is to effectively estimate the target-specific point feature on $(\hat{x}_{t+1}, \hat{y}_{t+1}, \hat{z}_{t+1})$. In the design of EVM, we use coordinate offsets as explicit voting signals for target center feature estimation. Specifically, we firstly calculate the coordinate offset between the estimated target center and each search seed. We then concatenate the coordinate offset with the search seed feature to obtain a candidate voting feature $f \in \mathbb{R}^{C+3}$, where C denotes the feature dimension. Suppose there are N search seeds with N corresponding candidate voting features $\{f_i\}_{i=1}^N$. The explicit target coordinate voting is formulated as:

$$\{\bar{f}_i\}_{i=1}^N = \text{MLP}(\{f_i\}_{i=1}^N), \quad \hat{f} = \text{MaxPool}(\{\bar{f}_i\}_{i=1}^N), \quad (4)$$

where $\{\bar{f}_i\}_{i=1}^N \in \mathbb{R}^{N \times C}$, and $\hat{f} \in \mathbb{R}^C$ is the final estimated target-specific feature for the estimated target center. The estimated feature \hat{f} is finally fed into a prediction head (i.e., MLP) for regressing the bounding box of target.

In the training stage, given a ground-truth target center location in a frame, we randomly sample diverse points around the ground-truth center. For stable training, the maximum distance between the sampled points and the ground-truth center should not be too large, and here we set it to 0.75 meters. During training, our EVM learns to estimate target-specific features of the sampled points that are effective for predicting the final bounding box. Note that the diverse sampled points can effectively mimic the noisy predictions of MPM, which makes our DMT more robust to noise in the predicted target track.

4.3. Loss function

Following [45], our training loss includes three components: classification loss, box-cloud loss, and regression

box loss. The former two losses enhance the target-specific feature extracted by the backbone, while the latter supervises the estimated 3D bounding box. In addition, we add a velocity loss for training the MPM (except for constant velocity model).

Seed-wise classification loss. Following [27], we note that only search area seeds located on the surface of a ground-truth target are useful in the EVM, and thus labeled as positives; all others are negatives. Therefore, a standard binary cross entropy loss L_{cla} is adopted to classify the search seeds.

BoxCloud loss. The BoxCloud features [45] in the search area are unknown in the inference stage, so we need to predict the 9D BoxCloud coordinate C_{bc} of objects in the search area, which is supervised by a smooth-L1 regression loss.

$$\mathcal{L}_{bc} = \frac{1}{\sum_i E_i} \sum_{i=1}^N \|C_{bc}^i - \hat{C}_{bc}^i\| \cdot E_i, \quad (5)$$

where \hat{C}_{bc} are ground-truth BoxCloud coordinates pre-calculated before training. E_i is a binary mask, which indicates whether the i -th point is inside an object BBox or not.

3D box regression loss. The final result of our network is to predict the 3D box parameters $C_{bbox} = \{\hat{x}, \hat{y}, \hat{z}, \hat{\theta}\}$. Following previous work, we adopt Huber (smooth-L1 loss) to supervise the regression.

$$\mathcal{L}_{bbox} = \|C_{bbox} - \hat{C}_{bbox}\|, \quad (6)$$

where \hat{C}_{bbox} is ground-truth bounding box of the target.

Velocity loss. For training a MPM, we hope the distance between the predicted center coordinates of the target and

the ground truth are as small as possible. In this paper, we use mean squared error loss \mathcal{L}_v for supervision:

$$\mathcal{L}_v = \|C_{cen}^{t+1} - \hat{C}_{cen}^{t+1}\|_2, \quad (7)$$

where $C_{cen}^{t+1} = (\hat{x}_{t+1}, \hat{y}_{t+1}, \hat{z}_{t+1})$ (see Eq. (3)) is the predicted target center coordinate at the $(t+1)$ -th frame and \hat{C}_{cen}^{t+1} is the corresponding ground-truth coordinate. Note that we firstly train MPM with \mathcal{L}_v , and then we use the following loss to train the backbone network, EVM and the prediction head:

$$L = \alpha L_{cla} + \beta L_{bc} + \gamma L_{bbox}, \quad (8)$$

where α , β , and γ are hyperparameters to balance their relationship. Here we set $\alpha = 0.2$, $\beta = 1.0$, $\gamma = 0.2$.

4.4. Implementation details

We follow previous 3D trackers [27, 45] to generate template and search point clouds in both training and testing stages. To fairly compare with recent trackers equipped with online detectors, we use the same target-specific search feature generation method in BAT [45], which makes the predictions of BAT and our DMT both based on the same augmented search features. In the proposed MPM, we use one LSTM layer with 50 hidden units as the motion predictor. The input tracklet length is set to 10, meaning that we use target states in the previous 10 frames for prediction. The model size of this LSTM model is about 50K, which is extremely light. The EVM is implemented as a three layer MLP with 256 hidden units, where the first two layers are followed with a 1-D batch normalization layer and a ReLU activation layer. We use the same backbone and the box prediction head as P2B [27] and BAT [45].

In the training stage, we firstly generate tracklet training data (i.e., each tracklet contains the target center coordinates in every 10 frames and the corresponding ground-truth target center coordinates in the next frame) to train the LSTM network. The batch size is set to the overall dataset size, and the learning rate and training epochs are respectively set to $1e-3$ and 8000. The whole training takes only 28 seconds on the car category of the KITTI dataset, which is efficient. After training the LSTM network in the offline manner, we use it for online testing without further modifications. The proposed DMT is trained for 60 epochs using Adam optimizer with a batch size of 100. The learning rate is initialized as $1e-3$ and decayed with 0.5 in every 5 epochs.

5. Experiments

We next present experiments on the KITTI and NuScenes datasets to demonstrate the efficacy of our lightweight 3D SOT model, DMT.

5.1. Dataset

The KITTI dataset [9] includes raw point clouds scanned by the Velodyne HDL-64E rotating 3D laser scanner and annotations for object instances in the form of 3D bounding boxes. The tailored dataset contains 21 outdoor scenes and 8 categories of targets. Following [27, 30, 33, 45], we generate tracklets and split the KITTI training set into three parts: scenes 00-16, scenes 17-18, and scenes 19-20 for training/valid/test set respectively since the annotations of the test set in KITTI are inaccessible. Furthermore, we also conduct experiments on the more challenging dataset NuScenes [5]. The NuScenes dataset includes 1000 outdoor scenes and 23 categories of objects with annotated 3D bounding boxes. Specifically, the NuScenes dataset contains 32302 frames on the car category, which is five times larger than the KITTI dataset. Following [45], the training set of NuScenes is used for training and the validation set is used for testing.

5.2. Evaluation metric

Following [27, 45], we apply One Pass Evaluation (OPE) [37] to measure Success and Precision of different approaches. For a predicted bounding box and a ground-truth bounding box, ‘‘Success’’ is defined using Area Under the Curve (AUC) for intersection over union (IOU) between them. ‘‘Precision’’ is defined as AUC for errors (The distance between the centers of two boxes from 0 to 2m).

5.3. Comparison with State-of-the-arts

We compare our network with the state-of-the-art methods: SC3D [1], its follow-up SC3D-RPN [41], FSiamese [47], 3DSiamRPN [8], P2B [27], MLVSNet [33], PTT [30], and BAT [45]. For a fair comparison, we use the same evaluation metrics. In this paper, the default setting of the MPM is a LSTM prediction model. Table 1 shows the success and precision of each network on the KITTI and NuScenes datasets. The success and precision values for other methods are those reported in their published papers [1, 8, 27, 30, 33, 41, 45, 47]. We first quantitatively evaluate our network on KITTI, and then extend the comparisons to NuScenes.

Comparisons on KITTI. Following [27, 45], we generate the search area centered on the previous result in the inference stage to meet the requirement of real scenarios. The results in Table 1 show that the proposed DMT outperforms other 3D trackers significantly. Specially, we first mix all categories together to test the average performance following previous trackers. The average performance of ours reaches 55.1, outperforming BAT by $\sim 4\%$ on Success, indicating the proposed DMT effectively explores the previous frames in an explicit way. Some qualitative results are given in Section 5.4. To demonstrate the generalizability for non-rigid object (Pedestrian) tracking, we compared

Table 1. Results of the Success and Precision of different 3D trackers with different categories on KITTI and NuScenes dataset. 'Ped' represents 'Pedestrian'.

	Dataset	KITTI					NuScenes				
	Category Frame Number	Car 6424	Ped 6088	Van 1248	Cyclist 308	Mean 14068	Car 32302	Trunk 8646	Trailer 2297	Bus 2215	Mean 45460
Success (%)	SC3D [10]	41.3	18.2	40.4	41.5	31.2	30.6	23.5	27.4	23.6	28.7
	SC3D-RPN [41]	36.3	17.9	-	43.2	-	-	-	-	-	-
	FSiamese [47]	37.1	16.2	-	47.0	-	-	-	-	-	-
	3DSiamRPN [8]	58.2	35.2	45.6	36.1	46.6	-	-	-	-	-
	P2B [27]	56.2	28.7	40.8	32.1	42.4	34.6	25.2	30.0	28.4	32.3
	MLVSNet [33]	56.0	34.1	52.0	34.3	45.7	-	-	-	-	-
	PTT [30]	67.8	44.9	43.6	37.2	55.1	-	-	-	-	-
	BAT [45]	60.5	42.1	52.4	33.7	51.2	36.8	28.6	31.8	30.2	34.7
	DMT	66.4	48.1	53.3	70.4	55.1	43.8	51.3	46.8	38.2	44.0
Precision (%)	SC3D [10]	57.9	37.8	47.0	70.4	48.5	35.9	24.8	24.8	21.8	32.5
	SC3D-RPN [41]	51.0	47.8	-	81.2	-	-	-	-	-	-
	FSiamese [47]	50.6	32.2	-	77.2	-	-	-	-	-	-
	3DSiamRPN [8]	76.2	56.2	52.8	49.0	64.9	-	-	-	-	-
	P2B [27]	72.8	49.6	48.4	44.7	60.0	37.6	25.2	26.7	27.6	34.2
	MLVSNet [33]	74.0	61.1	61.4	44.5	66.6	-	-	-	-	-
	PTT [30]	81.8	72.0	52.5	47.3	74.2	-	-	-	-	-
	BAT [45]	77.7	70.1	67.0	45.4	72.8	39.5	28.4	30.5	29.5	36.4
	DMT	79.4	77.9	65.6	92.6	75.8	48.3	51.1	40.3	31.9	47.3

with other trackers on Pedestrian and Cyclist. For Pedestrian, we can observe that DMT outperforms BAT and PTT by $\sim 8\%$ and $\sim 6\%$ on Precision respectively, indicating the effectiveness of our tracking pipeline. Amazingly, DMT outperforms BAT and PTT by a large margin for the cyclist category, achieving about $\sim 47\%/\sim 45\%$ improvement on Precision. This phenomenon can be explained as follows: 1) The amount of training and testing samples are extremely small; 2) Our method DMT is more robust to interference with similar objects in the search area. The visualized results are shown in Fig. 3. This also demonstrates that our method can achieve better performance, especially when having less data compared with BAT.

Comparisons on NuScenes. For the car category, DMT reaches the best performance of 43.8/48.3 on Success/Precision, exceeding the performance of current state-of-the-art method BAT [45] by $\sim 7\%/\sim 9\%$ respectively. Notably, for the truck and trailer categories, DMT achieves about $\sim 23\%$ and 20% improvements over BAT on Precision, which demonstrates that our motion guided pipeline is more effective especially on the more challenging dataset. Moreover, for the bus category which has the smallest training samples, our DMT still outperforms BAT by a large margin of 8% in terms of the Success metric. Compared with the baseline method BAT, the performance of our DMT shows significant improvements ($\sim 10\%$ on average)

in terms of all categories. Note that PTT/MLVSNet did not present results on NuScenes in their papers.

5.4. Results visualization

According to the different categories and difficulties of the targets, we select and visualize some advantageous cases of our DMT in Fig. 3. Four frames sorted by time from a full sequence are selected from the cyclist and car category, respectively. For the cyclist target, the point clouds of the target and the tracked results are shown on the top of Fig. 3. In this example, BAT tracks the cyclist wrongly when there are two similar cyclists in the surrounding area. Our method can track the target accurately and tightly, indicating our method is more robust to the complex scenarios. Furthermore, we display the tracked results on the car category, which is shown in the bottom of Fig. 3. Here BAT fails in the extremely sparse scenes (fewer than 10 points), but our DMT works well, which shows that our proposed method is indeed robust to point sparsity.

6. Discussion

In this section, we analyze the effectiveness of important modules in our DMT, including both the motion prediction module (MPM) and the explicit voting module (EVM). The robustness test and computational cost are also analyzed.

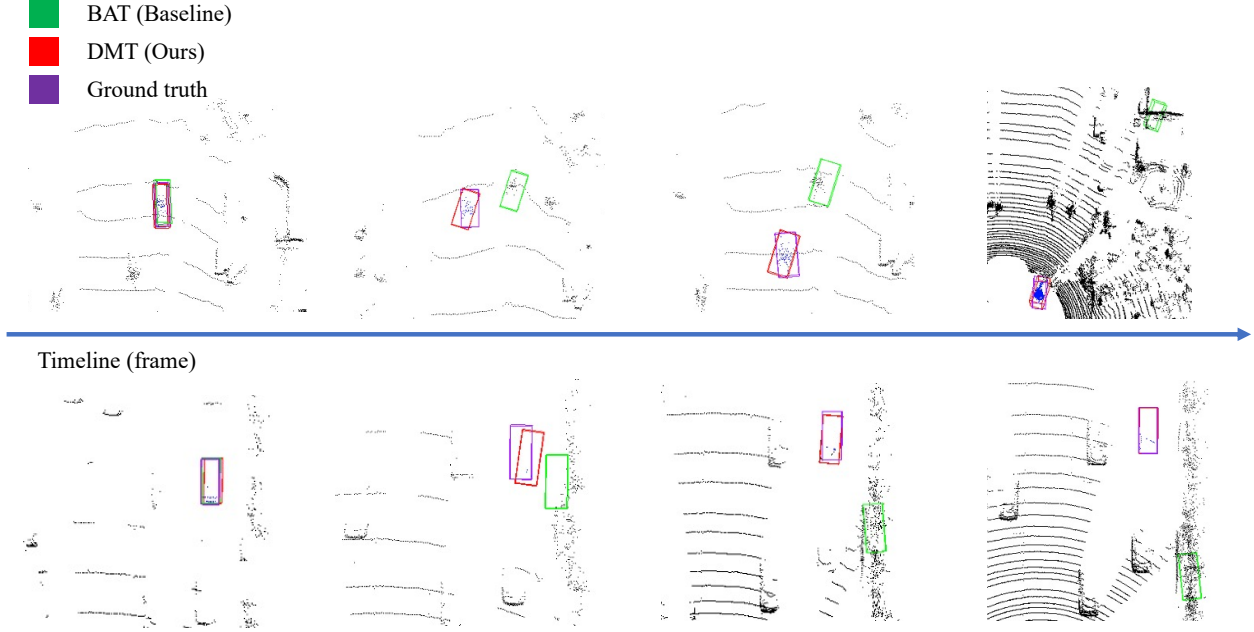


Figure 3. Visualizations of example results of DMT compared with BAT. The point clouds of tracked objects are shown in blue. (Top) shows results for test instances from the cyclist category. There are two cyclists in a neighboring area, and our DMT can maintain the correct track while BAT drifts to the wrong object. (Bottom) shows results for test instances from the car category. Although the point clouds are extremely sparse (< 10 points), our DMT still tracks the object.

6.1. Ablation studies of DMT components

Method	MP module	EV module	Success	Precision
BAT [45]			60.5	77.7
MP3-T-MP	✓		-	37.0
MP3-T-EV		✓	54.0	64.1
MP3-Tracking	✓	✓	66.4	79.4

Table 2. Ablation studies of motion prediction module and explicit voting module on KITTI-Car.

We first conduct an ablation study on the necessity of the EVM and MPM. All studies are conducted on KITTI-Car for convenience. We remove the EVM and the MPM in our network one by one, which is denoted as DMT_MP and DMT_EV. Both variations have the same structure as DMT except for the removed module. The baseline model is BAT. The results are shown in Table. 2.

We obtain four conclusions from these results. (1) The potential target center estimated by the MPM is extremely inaccurate, only reaching 37% on Precision. Note that the MPM in our network cannot regress the orientation of target, and thus we cannot compute the Success value. (2) The precision without EVM is 37% (DMT_MP), and with EVM is 79.4% (DMT). Thus this proves EVM can estimate the accurate target-specific point feature to further refine the prediction of MPM. (3) Comparing DMT_EV with BAT,

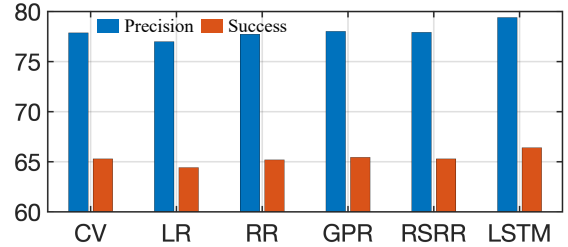


Figure 4. Comparison of using various regression or prediction models as our motion prediction module on KITTI-Car.

the performance of DMT_EV degrades about 6%/13% in terms of Success/Precision. This is consistent with our expectation that we use a simpler explicit voting module, removing the complicated RPN module. (4) Our full pipeline achieves the best performance, which demonstrates the two modules are mutually beneficial and necessary. In addition, even if the MPM provides inaccurate results, DMT achieves the satisfactory performance thanks to the explicit voting module.

6.2. The choice of motion prediction module

In Fig. 4, we compare various types of motion prediction models on KITTI-Car. The compared models include Constant Velocity (CV), Linear Regression (LR), Ridge Regression (RR), Gaussian Process Regression (GPR), RanSac

with Ridge Regression (RSRR) and LSTM models. For LR, RR, GPR and RSRR, we train them in the same way with the LSTM model, i.e., using the same sampled tracklets from the training data in KITTI-Car for offline training. These models are then applied for motion prediction during online testing without further updating. In Fig. 4, the differences among various models are not significant, which implies the our DMT is not sensitive to the MPM selection. This is because our EVM is trained to predict GT bounding boxes from diverse sampled locations in the training stage, which makes it more robust to predict the target bounding box from the noisily predicted target center locations. The sequence-to-sequence prediction LSTM model achieves the best Precision (79.4%) and Success (66.4%) due to its better sequence modelling ability.

6.3. Template generation strategy

We next explore the performance of our DMT performance with four template generation strategies following [45], including “the first ground-truth”, “the previous result”, “the first ground-truth and previous result”, and “all previous results”. Table 3 shows results of Success/Precision with different settings for different trackers on KITTI-Car. DMT achieves the best performance regardless of the used strategy. For the “all previous” setting, P2B, BAT and our DMT all report degraded results since these trackers did not train the networks using all previous results for efficiency, while SC3D did. Despite this, DMT still beats BAT by the largest margin ($\sim 8\%$) under the “all previous” setting. This suggests that DMT better utilizes motion cues from previous predictions compared with BAT.

Table 3. Different strategies for template generation. 3D trackers are evaluated on KITTI-Car.

	Method	The First GT	Previous result	First & Previous	All Previous
Success	SC3D [10]	31.6	25.7	34.9	41.3
	P2B [27]	46.7	53.1	56.2	51.4
	BAT [45]	51.8	59.2	60.5	55.8
	DMT(Ours)	54.3	63.8	66.4	63.5
Precision	SC3D [10]	44.4	35.1	49.8	57.9
	P2B [27]	59.7	68.9	72.8	66.8
	BAT [45]	65.5	75.6	77.7	71.4
	DMT(Ours)	67.2	76.7	79.4	75.9

6.4. Values of sampling distance analysis

In this section, we explore the network performance with different distances between the sampled points and the ground-truth center. As pointed in Section “Explicit voting module”, the distance should be not large for stable training. Thus we conduct experiments on KITTI-Car choosing

the distance values from 0.65 to 0.95. As shown in Table 4, the performance of DMT reaches the peak with a distance value of 0.75. When the distance expands to 0.95, the performance steadily degrades. This implies the distances between sampled points and the ground-truth center is still a little large so that some outliers are picked. On the other hand, the network performance drops when the distance is set to 0.65. Thus, in this paper, we fix the values to 0.75 for the best performance.

Distance	Success	Precision
0.65	64.0	77.0
0.75	66.4	79.4
0.85	63.0	77.5
0.95	63.0	76.8

Table 4. Sampling distance analysis for DMT. We evaluate DMT on KITTI-Car.

6.5. Number of sampled training points

In the practical implementation, we sample various points around the ground-truth target center to mimic motion predictions during the online tracking process. In this section, we study how the number of sampled points affects final tracking performance. Specifically, we vary the number of sampled points and report the corresponding performance in Table 5 on KITTI-Car. We discover that sampling dense points (i.e., 64) leads to better performance, owing to the dense sampling providing more comprehensive cases for learning a more robust EVM. We also notice that the performance is not saturated, implying that better performance can be obtained by sampling a larger number of points.

Num	Success	Precision
8	61.1	75.0
16	62.2	75.7
32	64.5	78.0
64	66.4	79.4

Table 5. Sampling point number analysis for DMT. We evaluate DMT on KITTI-Car.

6.6. Robustness test for object motion patterns

To better demonstrate the effectiveness of DMT on complex motion patterns, Fig. 5(a) shows the comparison of our DMT and BAT on tracklets with different motion complexity. Here motion complexity is defined as the average error of a simple constant velocity model. Our method still performs better than the RPN-based 3D tracker BAT when the motion complexity increases, which demonstrates the

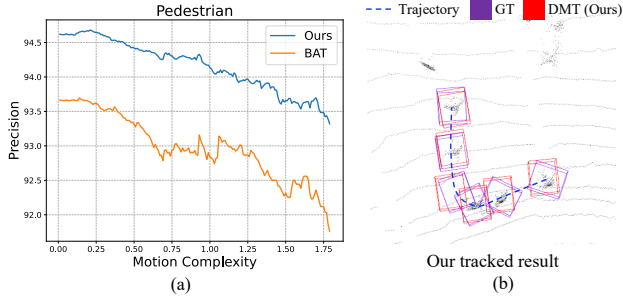


Figure 5. (a) Comparison of BAT and our DMT under various motion complexity on KITTI-Pedestrian. (b) Example results of DMT for complex motion patterns.

robustness of our method to complicated motion patterns. The reason for our robustness is that we randomly sample diverse points when training the EVM, which makes our method more effectively handle various motion patterns. We also visualize one tracklet of a pedestrian having a complex trajectory in Fig. 5(b), and DMT can track the target accurately despite the complicated motion pattern.

6.7. Computational cost analysis

In this section, we analyze the required computational resources of different 3D trackers in terms of the number of parameters, floating point operations (FLOPs) and running speed. For a fair comparison, here we test all frames of the KITTI-Car on a single NVIDIA 3090 GPU. As shown in Table 6, our method uses less time per frame with fewer FLOPs compared with other trackers. Notably, despite the fact that our network includes an LSTM model, the number of parameters of our model are the same as P2B, while our model is significantly faster (57% improvement in FPS) and simpler (36% improvement in FLOPs). Besides, the running time and floating point operations of DMT reaches 71.5 FPS and 2.98G, respectively. All results are better than BAT, MLVSNet and PTT, demonstrating that our method is faster, simpler, and lighter. The reason for this is that we design a detector-free strategy instead of the RPN module.

Table 6. Computational cost requirements of different 3D single object trackers on KITTI-Car.

Method	Modality	Params	FLOPs	FPS
SC3D [10]	LiDAR	-	-	1.8
FSiamese [47]	LiDAR+RGB	-	-	4.9
3DSiamRPN [8]	LiDAR	-	-	20.8
P2B [27]	LiDAR	5.4M	4.65G	45.5
MLVSNet [33]	LiDAR	7.6M	-	70.0
PTT [30]	LiDAR	-	-	40
BAT [45]	LiDAR	5.9M	3.05G	68.0
DMT(Ours)	LiDAR	5.4M	2.98G	71.5

7. Conclusion

In this paper, we propose DMT, a novel lightweight and detector-free network for 3D single object tracking. We design a motion prediction module for predicting a potential target center, explicitly leveraging spatial-temporal correlations from previous frames to explore the prior knowledge. In addition, we propose a simplified voting module to regress accurate 3D box with the guidance of the potential target center. Experiments show that our method DMT is lighter, faster, simpler and improves the tracking performance over state-of-the-art methods significantly. According to discussions on experimental results, the explicit voting module based on a potential target center is our method’s shining point. We hope that our work will inspire more investigation of the lightweight and detector-free 3D single object trackers.

References

- [1] Panos Achlioptas, Olga Diamanti, Ioannis Mitliagkas, and Leonidas Guibas. Learning representations and generative models for 3d point clouds. In *International conference on machine learning*, pages 40–49. PMLR, 2018. 1, 6
- [2] Alireza Asvadi, Pedro Girao, Paulo Peixoto, and Urbano Nunes. 3d object tracking using rgb and lidar data. In *2016 IEEE 19th International Conference on Intelligent Transportation Systems (ITSC)*, pages 1255–1260. IEEE, 2016. 3
- [3] Luca Bertinetto, Jack Valmadre, Joao F Henriques, Andrea Vedaldi, and Philip HS Torr. Fully-convolutional siamese networks for object tracking. In *European conference on computer vision*, pages 850–865. Springer, 2016. 2
- [4] Adel Bibi, Tianzhu Zhang, and Bernard Ghanem. 3d part-based sparse tracker with automatic synchronization and registration. In *Proceedings of the IEEE Conference on Computer Vision and Pattern Recognition*, pages 1439–1448, 2016. 3
- [5] Holger Caesar, Varun Bankiti, Alex H Lang, Sourabh Vora, Venice Erin Liong, Qiang Xu, Anush Krishnan, Yu Pan, Giancarlo Baldan, and Oscar Beijbom. nuscenes: A multi-modal dataset for autonomous driving. In *Proceedings of the IEEE/CVF conference on computer vision and pattern recognition*, pages 11621–11631, 2020. 2, 6
- [6] Andrew I Comport, Éric Marchand, and François Chaumette. Robust model-based tracking for robot vision. In *2004 IEEE/RSJ International Conference on Intelligent Robots and Systems (IROS)(IEEE Cat. No. 04CH37566)*, volume 1, pages 692–697. IEEE, 2004. 1
- [7] Yubo Cui, Zheng Fang, and Sifan Zhou. Point siamese network for person tracking using 3d point clouds. *Sensors*, 20(1):143, 2020. 3
- [8] Zheng Fang, Sifan Zhou, Yubo Cui, and Sebastian Scherer. 3d-siamrpn: An end-to-end learning method for real-time 3d single object tracking using raw point cloud. *IEEE Sensors Journal*, 21(4):4995–5011, 2020. 3, 6, 7, 10
- [9] Andreas Geiger, Philip Lenz, and Raquel Urtasun. Are we ready for autonomous driving? the kitti vision benchmark

- suite. In *2012 IEEE conference on computer vision and pattern recognition*, pages 3354–3361. IEEE, 2012. 2, 6
- [10] Silvio Giancola, Jesus Zarzar, and Bernard Ghanem. Leveraging shape completion for 3d siamese tracking. In *Proceedings of the IEEE/CVF Conference on Computer Vision and Pattern Recognition*, pages 1359–1368, 2019. 1, 3, 7, 9, 10
- [11] Qing Guo, Wei Feng, Ce Zhou, Rui Huang, Liang Wan, and Song Wang. Learning dynamic siamese network for visual object tracking. In *Proceedings of the IEEE international conference on computer vision*, pages 1763–1771, 2017. 2
- [12] Kaiming He, Xiangyu Zhang, Shaoqing Ren, and Jian Sun. Deep residual learning for image recognition. In *Proceedings of the IEEE conference on computer vision and pattern recognition*, pages 770–778, 2016. 2
- [13] Sepp Hochreiter and Jürgen Schmidhuber. Long short-term memory. *Neural computation*, 9(8):1735–1780, 1997. 4
- [14] Hou-Ning Hu, Qi-Zhi Cai, Dequan Wang, Ji Lin, Min Sun, Philipp Krahenbuhl, Trevor Darrell, and Fisher Yu. Joint monocular 3d vehicle detection and tracking. In *Proceedings of the IEEE/CVF International Conference on Computer Vision*, pages 5390–5399, 2019. 3
- [15] Ugur Kart, Joni-Kristian Kamarainen, and Jiri Matas. How to make an rgb-d tracker? In *Proceedings of the European Conference on Computer Vision (ECCV) Workshops*, pages 0–0, 2018. 3
- [16] Ugur Kart, Alan Lukezic, Matej Kristan, Joni-Kristian Kamarainen, and Jiri Matas. Object tracking by reconstruction with view-specific discriminative correlation filters. In *Proceedings of the IEEE/CVF Conference on Computer Vision and Pattern Recognition*, pages 1339–1348, 2019. 3
- [17] B Ravi Kiran, Ibrahim Sobh, Victor Talpaert, Patrick Mannion, Ahmad A Al Sallab, Senthil Yogamani, and Patrick Pérez. Deep reinforcement learning for autonomous driving: A survey. *IEEE Transactions on Intelligent Transportation Systems*, 2021. 1
- [18] Bo Li, Wei Wu, Qiang Wang, Fangyi Zhang, Junliang Xing, and Junjie Yan. Siamrpn++: Evolution of siamese visual tracking with very deep networks. In *Proceedings of the IEEE/CVF Conference on Computer Vision and Pattern Recognition*, pages 4282–4291, 2019. 2, 3
- [19] Bo Li, Junjie Yan, Wei Wu, Zheng Zhu, and Xiaolin Hu. High performance visual tracking with siamese region proposal network. In *Proceedings of the IEEE conference on computer vision and pattern recognition*, pages 8971–8980, 2018. 1
- [20] Bo Li, Junjie Yan, Wei Wu, Zheng Zhu, and Xiaolin Hu. High performance visual tracking with siamese region proposal network. In *Proceedings of the IEEE conference on computer vision and pattern recognition*, pages 8971–8980, 2018. 2, 3
- [21] Yuan Liu, Ruoteng Li, Yu Cheng, Robby T Tan, and Xiubao Sui. Object tracking using spatio-temporal networks for future prediction location. In *European Conference on Computer Vision*, pages 1–17. Springer, 2020. 3
- [22] Wenjie Luo, Bin Yang, and Raquel Urtasun. Fast and furious: Real time end-to-end 3d detection, tracking and motion forecasting with a single convolutional net. In *Proceedings of the IEEE conference on Computer Vision and Pattern Recognition*, pages 3569–3577, 2018. 1
- [23] Eiji Machida, Meifen Cao, Toshiyuki Murao, and Hiroshi Hashimoto. Human motion tracking of mobile robot with kinect 3d sensor. In *2012 Proceedings of SICE Annual Conference (SICE)*, pages 2207–2211. IEEE, 2012. 1
- [24] Aljoša Osep, Wolfgang Mehner, Markus Mathias, and Bastian Leibe. Combined image-and world-space tracking in traffic scenes. In *2017 IEEE International Conference on Robotics and Automation (ICRA)*, pages 1988–1995. IEEE, 2017. 3
- [25] Abhishek Patil, Srikanth Malla, Haiming Gang, and Yi-Ting Chen. The h3d dataset for full-surround 3d multi-object detection and tracking in crowded urban scenes. In *2019 International Conference on Robotics and Automation (ICRA)*, pages 9552–9557. IEEE, 2019. 3
- [26] Charles R Qi, Or Litany, Kaiming He, and Leonidas J Guibas. Deep hough voting for 3d object detection in point clouds. In *Proceedings of the IEEE/CVF International Conference on Computer Vision*, pages 9277–9286, 2019. 1
- [27] Haozhe Qi, Chen Feng, Zhiguo Cao, Feng Zhao, and Yang Xiao. P2b: Point-to-box network for 3d object tracking in point clouds. In *Proceedings of the IEEE/CVF Conference on Computer Vision and Pattern Recognition*, pages 6329–6338, 2020. 1, 2, 3, 4, 5, 6, 7, 9, 10
- [28] Branko Ristic, Sanjeev Arulampalam, and Neil Gordon. *Beyond the Kalman filter: Particle filters for tracking applications*. Artech house, 2003. 1
- [29] Samuel Scheidegger, Joachim Benjaminsson, Emil Rosenberg, Amrit Krishnan, and Karl Granström. Mono-camera 3d multi-object tracking using deep learning detections and pmbm filtering. In *2018 IEEE Intelligent Vehicles Symposium (IV)*, pages 433–440. IEEE, 2018. 3
- [30] Jiayao Shan, Sifan Zhou, Zheng Fang, and Yubo Cui. Ptt: Point-track-transformer module for 3d single object tracking in point clouds. *arXiv preprint arXiv:2108.06455*, 2021. 1, 3, 4, 6, 7, 10
- [31] Jiaming Sun, Yiming Xie, Siyu Zhang, Linghao Chen, Guofeng Zhang, Hujun Bao, and Xiaowei Zhou. You don’t only look once: Constructing spatial-temporal memory for integrated 3d object detection and tracking. In *Proceedings of the IEEE/CVF International Conference on Computer Vision*, pages 3185–3194, 2021. 3
- [32] Jianren Wang and Yihui He. Motion prediction in visual object tracking. In *2020 IEEE/RSJ International Conference on Intelligent Robots and Systems (IROS)*, pages 10374–10379. IEEE, 2020. 3
- [33] Zhoutao Wang, Qian Xie, Yu-Kun Lai, Jing Wu, Kun Long, and Jun Wang. Mlvsnet: Multi-level voting siamese network for 3d visual tracking. In *Proceedings of the IEEE/CVF International Conference on Computer Vision*, pages 3101–3110, 2021. 1, 3, 4, 6, 7, 10
- [34] Xinshuo Weng, Jianren Wang, David Held, and Kris Kitani. 3d multi-object tracking: A baseline and new evaluation metrics. In *2020 IEEE/RSJ International Conference on Intelligent Robots and Systems (IROS)*, pages 10359–10366. IEEE, 2020. 3

- [35] Xinshuo Weng, Yongxin Wang, Yunze Man, and Kris M Kitani. Gnn3dmot: Graph neural network for 3d multi-object tracking with 2d-3d multi-feature learning. In *Proceedings of the IEEE/CVF Conference on Computer Vision and Pattern Recognition*, pages 6499–6508, 2020. 3
- [36] Hai Wu, Qing Li, Chenglu Wen, Xin Li, Xiaoliang Fan, and Cheng Wang. Tracklet proposal network for multi-object tracking on point clouds. In Zhi-Hua Zhou, editor, *Proceedings of the Thirtieth International Joint Conference on Artificial Intelligence, IJCAI-21*, pages 1165–1171. International Joint Conferences on Artificial Intelligence Organization, 8 2021. Main Track. 3
- [37] Yi Wu, Jongwoo Lim, and Ming-Hsuan Yang. Online object tracking: A benchmark. In *Proceedings of the IEEE conference on computer vision and pattern recognition*, pages 2411–2418, 2013. 6
- [38] Yan Xia, Yusheng Xu, Shuang Li, Rui Wang, Juan Du, Daniel Cremers, and Uwe Stilla. Soe-net: A self-attention and orientation encoding network for point cloud based place recognition. In *Proceedings of the IEEE/CVF Conference on Computer Vision and Pattern Recognition*, pages 11348–11357, 2021. 1
- [39] Yan Xia, Yusheng Xu, Cheng Wang, and Uwe Stilla. Vpc-net: Completion of 3d vehicles from mls point clouds. *ISPRS Journal of Photogrammetry and Remote Sensing*, 174:166–181, 2021. 1
- [40] Tianyu Yang and Antoni B Chan. Learning dynamic memory networks for object tracking. In *Proceedings of the European conference on computer vision (ECCV)*, pages 152–167, 2018. 2
- [41] Jesus Zarzar, Silvio Giancola, and Bernard Ghanem. Efficient bird eye view proposals for 3d siamese tracking. *arXiv preprint arXiv:1903.10168*, 2019. 6, 7
- [42] Lichao Zhang, Abel Gonzalez-Garcia, Joost van de Weijer, Martin Danelljan, and Fahad Shahbaz Khan. Learning the model update for siamese trackers. In *Proceedings of the IEEE/CVF International Conference on Computer Vision*, pages 4010–4019, 2019. 2
- [43] Wenwei Zhang, Hui Zhou, Shuyang Sun, Zhe Wang, Jianping Shi, and Chen Change Loy. Robust multi-modality multi-object tracking. In *Proceedings of the IEEE/CVF International Conference on Computer Vision*, pages 2365–2374, 2019. 3
- [44] Zhipeng Zhang and Houwen Peng. Deeper and wider siamese networks for real-time visual tracking. In *Proceedings of the IEEE/CVF Conference on Computer Vision and Pattern Recognition*, pages 4591–4600, 2019. 2, 3
- [45] Chaoda Zheng, Xu Yan, Jiantao Gao, Weibing Zhao, Wei Zhang, Zhen Li, and Shuguang Cui. Box-aware feature enhancement for single object tracking on point clouds. In *Proceedings of the IEEE/CVF International Conference on Computer Vision*, pages 13199–13208, 2021. 1, 2, 3, 4, 5, 6, 7, 8, 9, 10
- [46] Xingyi Zhou, Vladlen Koltun, and Philipp Krähenbühl. Tracking objects as points. In *European Conference on Computer Vision*, pages 474–490. Springer, 2020. 3
- [47] Hao Zou, Jinhao Cui, Xin Kong, Chujuan Zhang, Yong Liu, Feng Wen, and Wanlong Li. F-siamese tracker: A frustum-based double siamese network for 3d single object tracking. In *2020 IEEE/RSJ International Conference on Intelligent Robots and Systems (IROS)*, pages 8133–8139. IEEE, 2020. 3, 6, 7, 10